applied sciences

MDPI

*Article*

# Flexural Behavior of a New Precast Insulation Mortar Sandwich Panel

**Mingshan Zhang [1,2], Weirong Feng [1,*], Kepeng Chen [2] and Benyue Li [2]**

[1] Center for Balance Architecture, Zhejiang University, Hangzhou 310028, China; zhangms@zuadr.com
[2] The Architectural Design & Research Institute of Zhejiang University Corporation Limited, Hangzhou 310028, China; ckp@zuadr.com (K.C.); lby@zuadr.com (B.L.)
* Correspondence: 22112223@zju.edu.cn

**Abstract:** This article introduces the experimental and analytical research results of two precast insulation mortar concrete sandwich panels (PIMSP) and two precast concrete composite panels as one-way slabs under bending load. Obtaining a prefabricated floor slab that can balance thermal insulation and structural performance can reduce material consumption and increase inter-story usage height. As the sandwich material for PIMSP, insulation mortar with a strength of 6 MPa was used. Truss-shaped shear connectors were used for shear force transfer. Then, finite element analysis was used to analyze and study the unidirectional flat plate model. The results showed that the tested PIMSP achieved a complete composite effect in the elastic stage and a semi-composite effect in the plastic stage. The PIMSP crack pattern resembles that of a precast concrete slab when utilized as a one-way slab. The load transfer capacity of truss-shaped shear connectors is relatively small, and it is mainly used as a connection between floors. Experiments have demonstrated that PIMSP panels can serve as a structural substitute for regular concrete floors in residential buildings.

**Keywords:** precast insulation mortar sandwich panels (PIMSP); shear connectors; finite element analysis (FEA); crack patterns; composites

check for updates

**Citation:** Zhang, M.; Feng, W.; Chen, K.; Li, B. Flexural Behavior of a New Precast Insulation Mortar Sandwich Panel. *Appl. Sci.* **2024**, *14*, 2071. https://doi.org/10.3390/app14052071

Academic Editor: Sang-Hyo Kim

Received: 26 January 2024
Revised: 25 February 2024
Accepted: 26 February 2024
Published: 1 March 2024

**Copyright:** © 2024 by the authors. Licensee MDPI, Basel, Switzerland. This article is an open access article distributed under the terms and conditions of the Creative Commons Attribution (CC BY) license (https://creativecommons.org/licenses/by/4.0/).

## 1. Introduction

Precast concrete sandwich panel (PCSP) was first prefabricated as a non-bearing system called "cladding panel", which comprised two thick internal and external concrete wythes designed as load- and non-bearing walls, respectively. PCSP is commonly used to construct the outer shell of several typical buildings, such as residential, commercial, and warehouse infrastructures [1–3]. As shown in Figure 1, a typical PCSP consists of two precast reinforced concrete layers (called wythes) separated by a layer of insulation and joined with connectors that penetrate the insulation layer [4–14]. To increase structural efficiency, various types of connectors (sometimes made of steel) can be used to promote composite behavior [15]. Pfeifer and Hanson [16,17] carried out experiments on small-scale concrete sandwich panels to study their flexural behavior. Different types of wythe reinforcement, shear connectors, and core thickness were used in their experiments. They concluded that the presence of edge ribs and the type of shear connectors significantly affect the failure load and the flexural behavior, respectively, of the panels.

There are many different types of sandwich panel insulation layer, such as polystyrene particles, foam concrete, and thermal insulation mortar. Insulation mortar is the term used to describe an insulation mortar composed mainly of fibers, expanded vitrified microspheres, and Portland cement [18]. The heat transfer coefficient usually varies between 0.07 and 0.085 $W/m^2 \cdot K$ after curing. Although it is less efficient in terms of heat transfer than particles made of polystyrene (between 0.03 and 0.05 $W/m^2 \cdot K$), it is less expensive and easier to build. Since different companies develop different formulas for insulation mortar, there is not a single, universal formula. The insulation mortar used in this paper was composed of fibers, fly ash, Portland cement, expanded vitrified microspheres, and polystyrene particles.

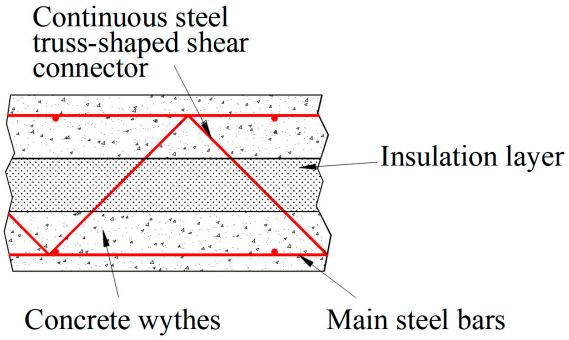


**Figure 1.** A partial cut of PCSP and steel truss-shaped shear connector.

PCSPs were used in this research as prefabricated floor slabs. Shear forces are transmitted along the vertical direction and are primarily impacted by bending loads in terms of structural stress. For shear force transfer, shear connectors were used. The quantity and quality of these connectors affect the composite connection effect they create, since they transfer shear force between the insulation layer and concrete wythes. Fengtao Bai [19] arranged shear connectors on a two-dimensional plane and found that higher shear stiffness of the connector can provide better composite behavior, and arranging shear connectors at the maximum slip position has a better effect on improving the structural response. Brandon Cox [20] conducted a large-scale flexible test and found that more shear connectors can provide better composite action. The truss-shaped shear connector used in this article is made up of two bent web bars that join the upper and lower chord bars to form a triangular cross-section, as seen in Figure 2 [21]. The height for each bent web bar was 100 mm, and the distance was 100 mm. The stiffness and strength of the connector play a major role in the panel's strength, and the insulation layer's thermal resistance affects the panel's general thermal resistance value.

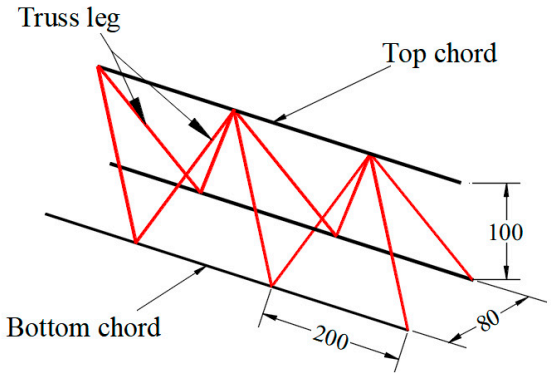


**Figure 2.** Details of steel truss-shaped shear connector design (all dimensions in mm).

Due to the varying properties of the sandwich material, the degree of connection between the various composite layers of the sandwich panel will have a significant impact on the final internal force distribution under bending loads. Depending on the degree of composite action achieved, a PCSP may be regarded as a fully composite, semi-composite or non-composite panel [22–25]. Up until they sustain damage, sandwich panels should be used and designed in accordance with the principle of maintaining integrity. The fully composite panel's steel bars and shear connectors will not sustain damage prior to the concrete experiencing compression failure. As seen in Figure 3a, its strain essentially stays linear along the thickness direction. A non-composite panel's upper and lower surfaces should have two distinct neutral axes, meaning that each panel is bent independently and that the strain changes with the thickness as seen in Figure 3c. In this instance, shear connectors are typically absent from sandwich panels. A sandwich panel is classified as semi-composite if its shear connector can only transfer a portion of the longitudinal shear force. In this instance, Figure 3b depicts the strain distribution along the sandwich panel's

thickness direction. The overall strain is nonlinear, but neither the upper nor lower concrete wythes have an independent neutral axis. At the same time, the concrete wythes slide relative to one another, but the shear connectors will not sustain damage.

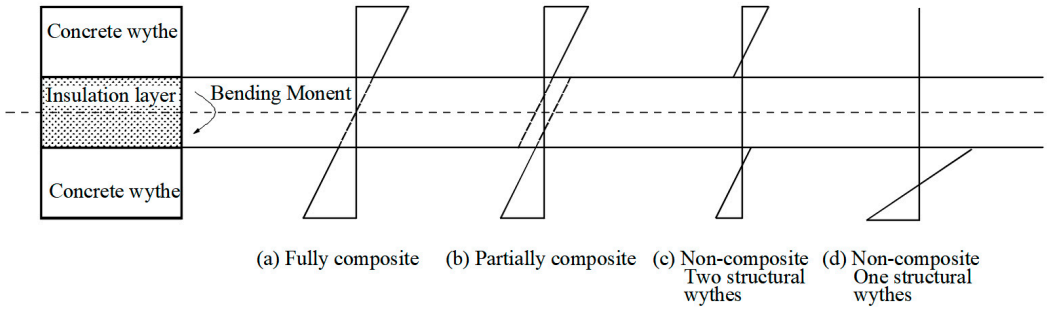


**Figure 3.** Bending stress distribution.

Numerous researchers have experimented with PCSP over the last thirty years. Einea et al. [3] found that full-scale concrete sandwich panel specimens exhibit more composite properties than small-sized specimens, [17] so using prototype panels in experiments can better reflect the results. Pessiki and Mlynarczyk's [26] research on PCSP shows that among the main components of PCSP, the solid concrete regions provided most of the composite action achieved in the panels. Benayoune et al. [8] studied the buckling behavior of PCSP made of polystyrene as an insulation layer under both unidirectional and bidirectional actions and found that the cracking mode of PCSP is very similar to that of traditional concrete slabs. Amran et al. [3] carried out an experimental and analytical study on the bending behavior of PCSP with foam concrete as the core. The findings demonstrated that sandwich panels and concrete panels had comparable fracture patterns. The sandwich panels achieved a complete composite in the elastic phase and a semi-composite in the plastic phase. Joseph et al. [17] found that the volume ratio and cross-sectional area ratio of the steel bars can affect the number and spacing of cracks in PCSP with Expanded Polystyrene (EPS) as the core. Because of the nonlinearity of sandwich panel materials, the unpredictability of shear connectors, and the interactions between various components, researchers must rely on experimental research to analyze the mechanical properties of sandwich panels under different conditions due to the complexity of PCSP analysis. It has been demonstrated by earlier experimental research and the impact of different variables that experimental research on the prototype panel is required when utilizing a novel material for the insulation layer and when utilizing distinct shear connectors.

The goal of this project is to create the PIMSP, a lightweight, easily assembled slab unit based on Chinese industrialized floor slabs. Insulation layers are typically laid on top of the concrete structure layer in China's modern residential floor slab construction technology, which not only makes construction inconvenient but also significantly lowers floor height. Furthermore, there is currently little research on floor slabs, and little attention is paid to the stress on wall panels in sandwich panels. Additionally, truss steel bars are not used as shear members in sandwich panels. Furthermore, the majority of current sandwich panel research focuses on the stress on wall panels, with relatively little research on floor slabs and even fewer using the truss-shaped shear connector mentioned above as shear members. Using sandwich panels as the structural layer, this article reduces the weight of each layer in the structure by 6% by adding insulating layers to two concrete surface layers, raising the layer height, and using less concrete.

## 2. Experimental Investigations

Two PIMSPs and two composite slabs were subjected to bending loads, designated JXB1, JXB2, and DHB1, DHB2, respectively. The experiment employed displacement loading up until failure, recording and observing the cracking modes and deformations at various stages of displacement increment [27].

### 2.1. Design of Panels

In order to test the bending effect of PIMSP under load and compare its differences with commonly used composite panels in engineering, two PIMSP and two concrete composite panels were designed and subjected to bending loads, named JXB1, JXB2 and DHB1, DHB2 respectively. Concrete composite panels are a type of pure concrete prefabricated floor slab used in engineering, serving as a control group between PIMSP and expected values. By comparing two PIMSPs, one can test the influence of the truss-shaped shear connectors and the insulation layer on the structural performance of the board. The experiment employed displacement loading up until failure, recording and observing the cracking modes and deformations at various stages of displacement increment.

As indicated in Figure 4 and Table 1, all panels were one-way slabs with a span of 3500 mm, a length of 3700 mm, and a width of 1200 mm. The difference between DHB1 and DHB2 is that DHB1 is 130 mm thick while DHB2 is 150 mm thick. JXB1 and DHB2 are different in that DHB2 is a composite slab poured with concrete, whereas JXB1 has an insulation layer composed of 20 mm thick insulation mortar. The difference between JXB1 and JXB2 is that JXB1 has two longitudinally arranged trusses, while JXB2 is not truss-equipped, which is used to compare the impact of trusses in PIMSP. The steel bar truss is connected to two layers of steel wire mesh and measures 300 mm from the upper chord bars to the outer edge of the plate, with a 600 mm spacing.

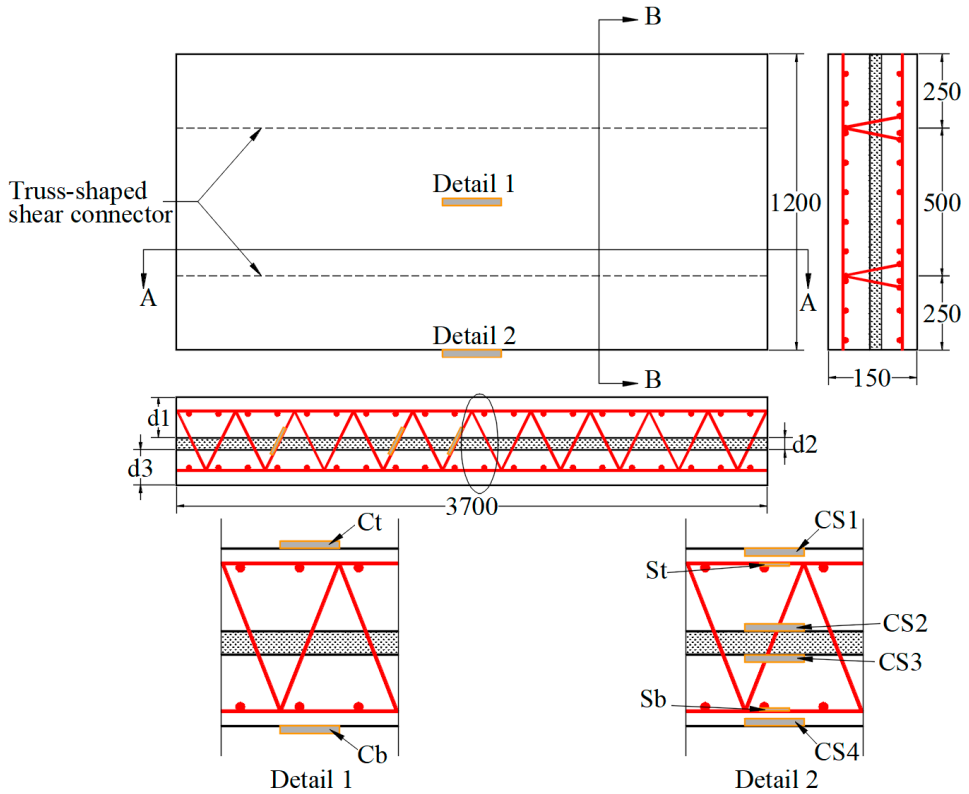


**Figure 4.** Details of the one-way slab PIMSP design (all dimensions in mm).

**Table 1.** Design sizes of the specimens.

| Name of Panel | Top Wythe $d_1$ (mm) | Insulation Layer $d_2$ (mm) | Bottom Wythe $d_3$ (mm) | L × b × d (mm × mm × mm) |
|---|---|---|---|---|
| DHB1 | 70 | 0 | 60 | 3700 × 1200 × 130 |
| DHB2 | 90 | 0 | 60 | 3700 × 1200 × 150 |
| JXB1 | 70 | 20 | 60 | 3700 × 1200 × 150 |
| JXB2 | 70 | 20 | 60 | 3700 × 1200 × 150 |

### 2.2. Material Properties and Specifications

For the insulation layer, the cement to water ratio was 1:0.5. For every 10 kg of cement, 0.003 cubic meters of polystyrene particles and 0.007 cubic meters of vitrified microspheres were added. Table 2 displays the insulation mortar's average cube strength, splitting tensile strength, and elastic modulus $E_c$ at 28 days.

**Table 2.** Concrete and mortar properties.

| Materials | $f_{cu}$ (MPa) | $f_t$ (MPa) | $E_c$ (GPa) |
|---|---|---|---|
| concrete | 48.28 | 3.71 | 29.8 |
| insulation mortar | 5.8 | 0.5 | 1.0 |

The properties of various types of steel bars are shown in Table 3, including yield strength, elastic modulus, and ultimate strength. Figures 5 and 6 show the testing process of concrete cube and steel bar, respectively.

**Table 3.** Steel properties.

| Steel Materials | Diameter (mm) | Yield Stress $f_y$ (MPa) | Stress at Ultimate Strength (MPa) | $E_s$ (GPa) |
|---|---|---|---|---|
| Steel reinforcement | 8 | 570 | 694 | 194 |
| truss chord | 10 | 531 | 690 | 214 |
| truss leg | 6 | 400 | 707 | 201 |



**Figure 5.** Concrete block being tested.



**Figure 6.** Steel reinforcement being tested.

### *2.3. Casting of PIMSP*

The combined thickness of the insulation layer and two concrete wythes make up the PIMSP design thickness. The steel truss in the middle serves as a connection, limiting the horizontal and vertical deformation between each layer. In Figure 7, the pouring procedure is displayed. The bottom concrete wythe was first poured and vibrated together with the mold on a vibration table. It initially set for two hours after it is poured, and then the insulation layer was poured right away. The insulation layer was manually smoothed since the insulation layer was only 20 mm thick and using a vibration table would harm the initially set concrete wythe. The top concrete was poured two days after the bottom concrete was poured. During the top concrete wythe pouring, a vibrating rod was utilized for single-point vibration and the surface was troweled manually. The top and bottom layers of steel mesh were poured inside the concrete. For each test model, two sets of three test blocks of concrete and insulation mortar were formed into cubes in batches. To hasten curing, the prepared specimen was placed in a damp area. To make sure the sample had enough moisture, these panel boards received a twice-daily spray of water. Then, 7 days after pouring, the formwork was removed and kept in the same conditions for 28 days.




**Figure 7.** Casting of PIMSP specimens.

### *2.4. Instrument Preparation and Monitoring*

The two types of electrical strain gauges (ESGs) were 3 and 80 mm in length. A total of 11 gauges were used for each sample in order to measure strain. One of the 3 mm-long strain gauges was positioned in the mid-span of the lower main reinforcement (Sb), another

in the mid-span of the upper main reinforcement (St), and three more were placed on the truss legs at various spans (TL1, TL2, TL3), as shown in Figure 8. On the mid-span surface of the panels, two 80 mm-long strain gauges were positioned, one at the top (Ct) and one at the bottom of the panel (Cb). To measure the neutral axis' movement under various loads, four more 80 mm-long gauges (CS1, CS2, CS3, CS4) were placed along the panel's side at evenly spaced heights, as shown in Figure 4.

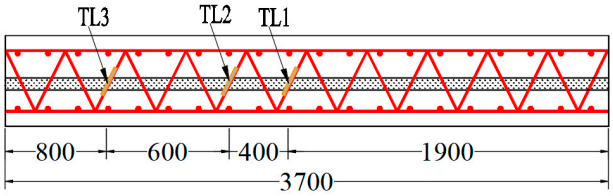


**Figure 8.** Location of ESGs on the truss legs (all dimensions in mm).

The location of the linear variable displacement transformers (LVDTs) is shown in Figure 9. Three LVDTs were installed in each panel; one was placed at the bottom of the mid-span and was primarily used to measure the deflection in the mid-span. To determine the loading point's deflection, there was also one at the bottom of each of the two loading points [28,29].

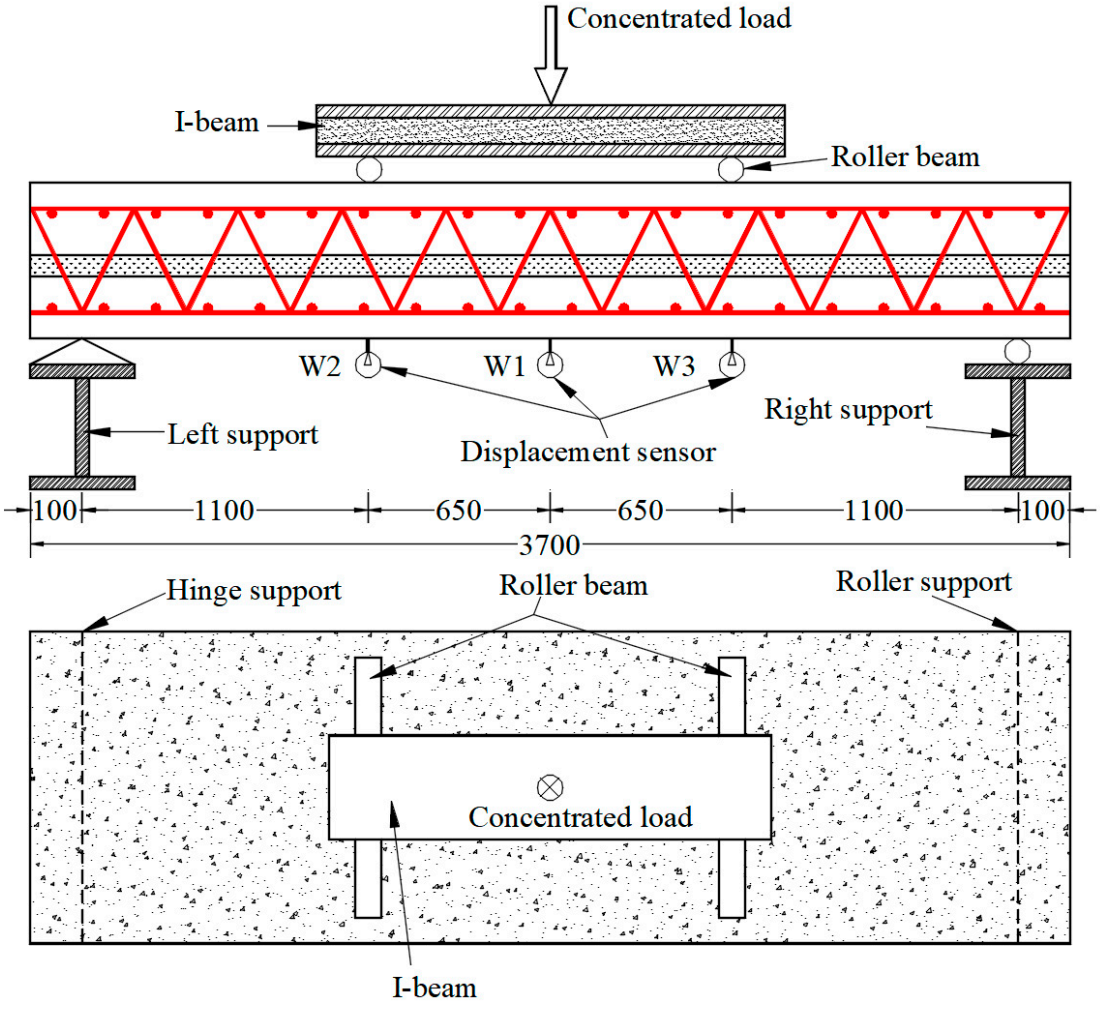


**Figure 9.** Details of the flexural test setup of specimens (all dimensions in mm).

A 1000 kN hydraulic servo testing machine was used to test the panels under bending load. As shown in Figures 9 and 10, the panel was placed horizontally with the support located on the short axis of the panel. Through an I-beam, a concentrated force from a hydraulic servo testing machine was transmitted to the two loading points. All panels were subjected to increasing bending loads until failure.

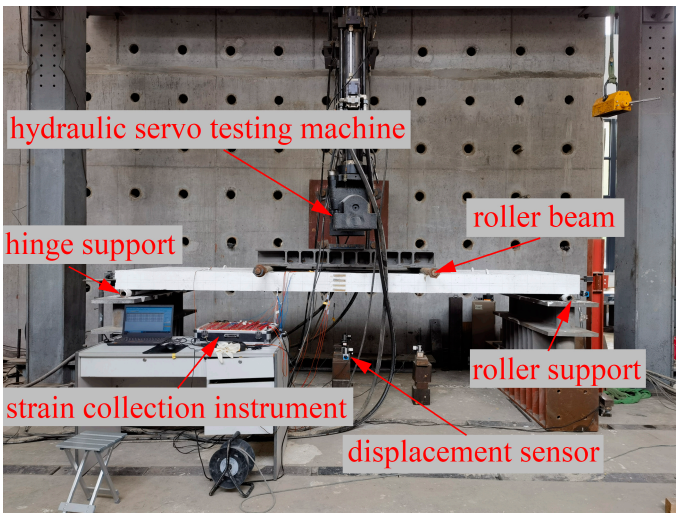


**Figure 10.** Details of the test system.

### *2.5. Test Procedure*

Before testing, the panel was painted white to make it easier to see any cracks. Grids measuring 100 by 100 mm were then drawn, with horizontal layering lines drawn at the borders. Displacement loading was chosen for loading due to the low estimated cracking load value and the notable effect of switching from force loading to displacement loading on numerical fluctuations. To make sure that the feedback load values and the instrument loading values were normal, we first applied a displacement of 0.5 mm. The applied displacement gradually increased by 1 mm until the panels fails. To automatically record the displacement and strain values of the steel bars and concrete at each phase, we used a strain collection instrument. In addition, crack patterns were noted and observed on the panel surface at each loading stage, and the crack width was measured.

## 3. Results and Discussion

Based on the deflection curve, cracking mode, load-strain relationship, strain variation across the slab depth, and yield load at failure, the experimental results were analyzed.

### *3.1. Load-Deflection Profile*

The load-deflection curve, which is derived from the specimen's static loading test, provides a thorough depiction of the sandwich panel's bending resistance performance and serves as a crucial foundation for examining the panel's mechanical performance. Figure 11 displays the mid-span load-deflection curves of the four test panels. According to the deflection curve, there is no evidence of cracking before the curve reaches the yield load, and it appears relatively linear. The curve can be used to determine the yield load's magnitude. The yield load of JXB1 is 25% greater than that of JXB2, 21% larger than that of DHB1, and only 2% smaller than that of DHB2. We examined the yield loads on the following four plates: DHB2 was greater than JXB1, which was greater than DHB1, which was more than JXB2. Before applying the yield load, we compared the deflection development speeds of four panels: the deflection development speeds of JXB1 and DHB2 were comparable, although they were not as fast as JXB2's. Out of the four panels, DHB1 exhibited the fastest deflection development speed.

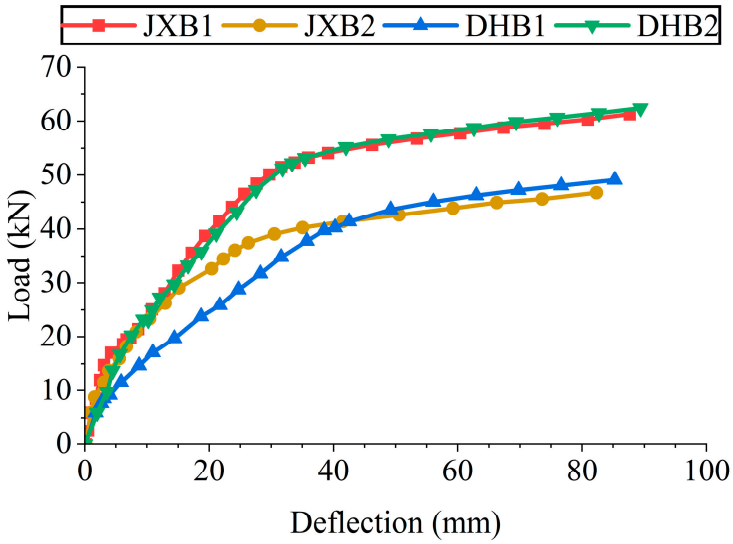


**Figure 11.** Load-deflection profile of mid-span for test panels.

Figure 12 displays the experimental panels' deflection contour lines along the slab span direction at different load stages. During the elastic stage, the deflection values of the four panels increase relatively uniformly. This proves that four test panels behave as one structural unit during loading, otherwise, the profile will show an irregular behavior [3].

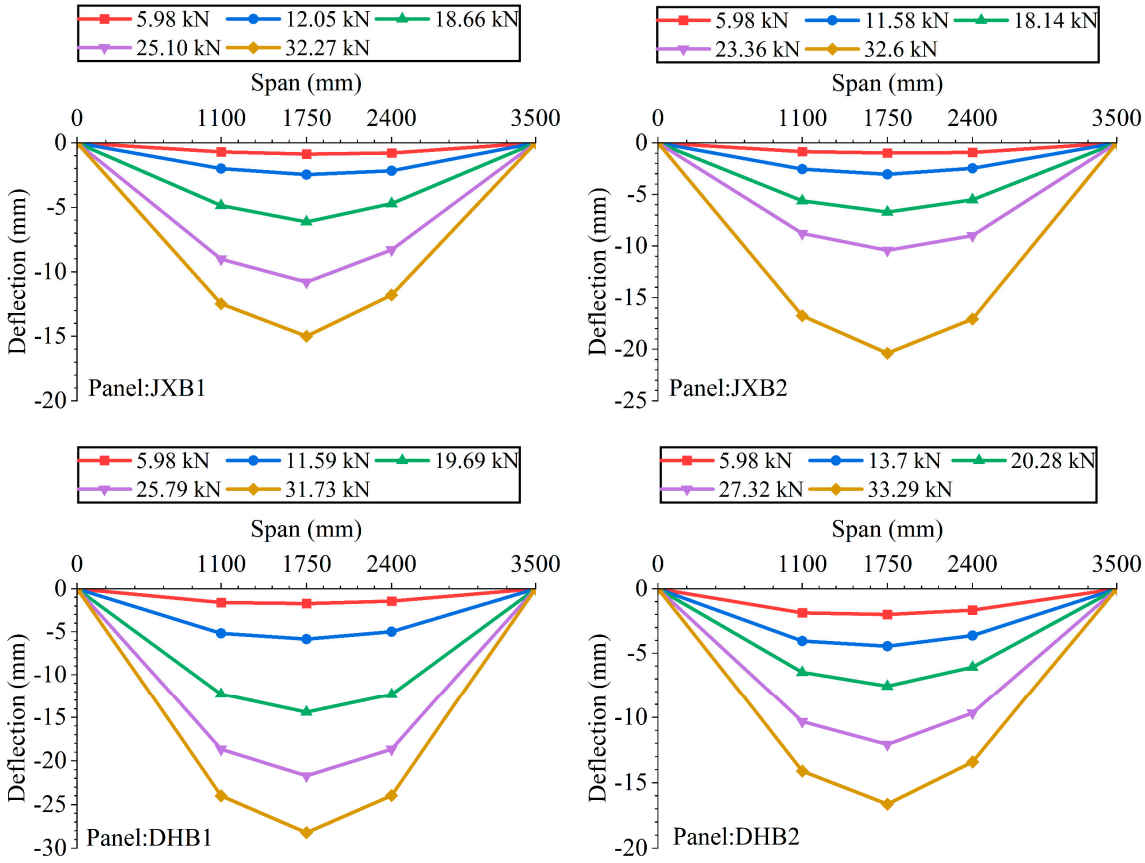


**Figure 12.** Deflection along the span of test panels at different load stages.

### *3.2. Load–Strain Relationship in Steel Bars*

The typical load–strain curve generated by the bottom reinforcement along the span direction of the four panels' faces is shown in Figure 13, where the timing of the crack occurrence can be clearly seen. At the initial stage of loading, the curve exhibits linear elasticity. JXB1 cracks at 37% of the ultimate load, JXB2 cracks at 37% of the ultimate load, DHB1 cracks at 19% of the ultimate load, and DHB2 cracks at 45% of the ultimate load.

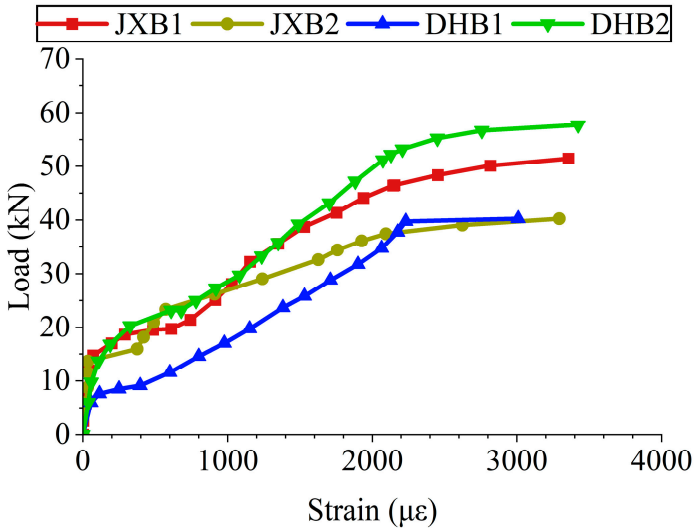


**Figure 13.** Load–strain in steel bars at the mid-span for the bottom wythe of test panels.

### *3.3. Load–Strain Relationship on Concrete Surface*

Figure 14 illustrates the load–strain curves for the top and bottom surfaces of the mid-span concrete surface. When the load is applied initially, the sandwich panel shows elasticity; as the load increases, plasticity sets in. The rise in concrete strain following cracking is proportionate to the increase in load, much like the load–deflection curve. When comparing the load–strain curves of the concrete on its top and bottom surfaces, one can observe that, during the elastic stage, the top and bottom strains are equal; however, once plasticity sets in, the bottom strains more than the top. The top concrete's maximum strain is 868 when looking at the plastic strain up to the yield load, yet the bottom concrete's strain gauge has failed.

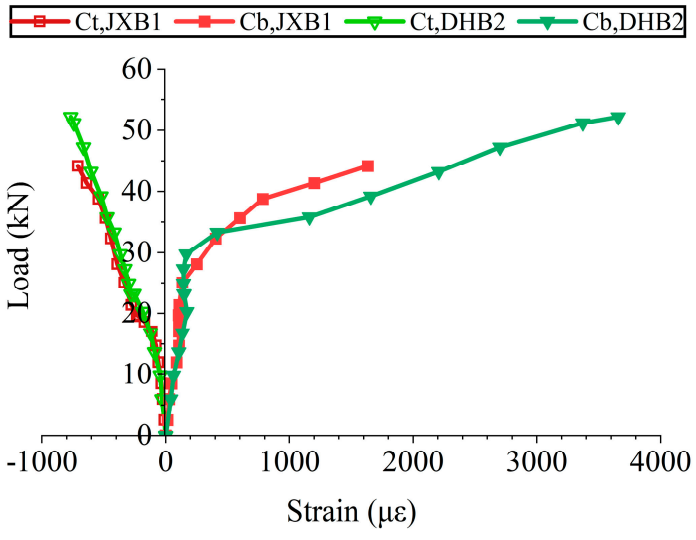


**Figure 14.** Load–strain on the top and bottom surfaces of concrete wythes for test panels.

Figure 15 displays the strain distribution along the PIMSP's thickness direction at different load stages. The curves are comparatively continuous during the elastic stage, but there is a discontinuity following cracking. The primary cause of this discontinuity is that the concrete's strength far outweighs the elasticity and strength of the material used for the insulation layer. As a result, discontinuous strain distribution occurs when the bottom concrete cracks and the insulating layer material is unable to transmit strain effectively. Although JXB2 lacks trusses, the strain distribution is comparable to that of JXB1, and no non-composite or approximate situation exists. Because there is no noticeable interlayer slip throughout the entire stress process, it can be attributed to the good bonding between the insulation layer and the surface layer.

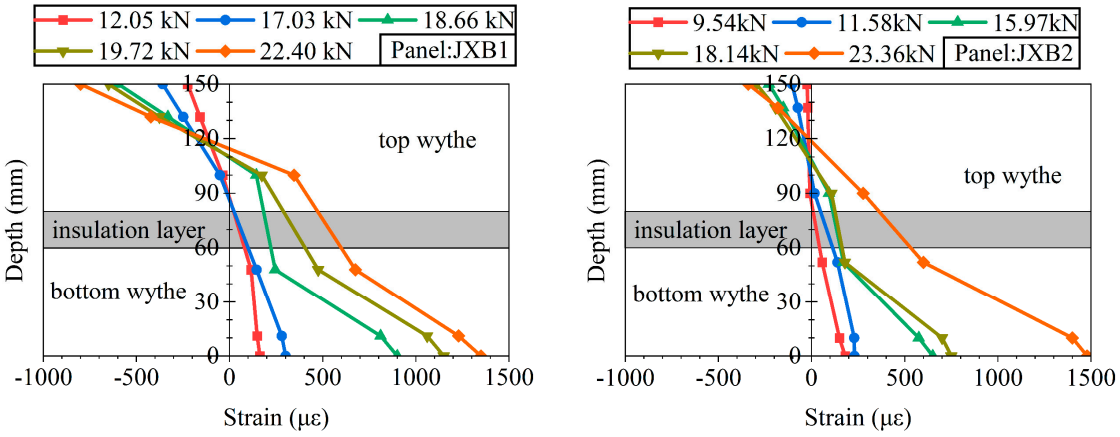


**Figure 15.** Strain distribution across the depth at different load stages for the tested panels.

### *3.4. Load–Strain Relationship in Truss Leg*

In its capacity as a connector, the truss serves as a force transmission structure between the upper and lower layers in addition to joining two concrete wythes and the sandwich layer. As depicted in Figure 8, the tension legs of the truss were pasted with strain gauges at different spans. Figure 16 illustrates that during the elastic stage, hardly any strain occurs. There is a period of compression strain following cracking. Tensile strain replaces compression strain as the load progressively rises.

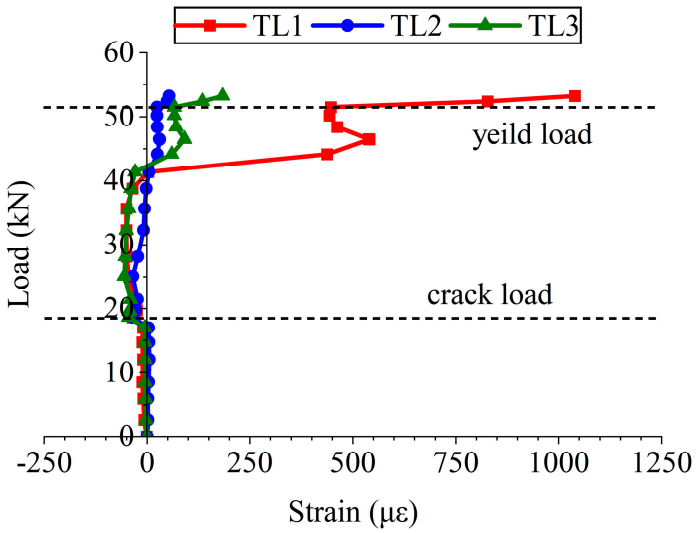


**Figure 16.** Load–strain on the truss legs at different spans for panel JXB1.

### *3.5. Cracking Patterns*

The load applied in the test is a constant displacement load until failure. We recorded the load and failure load at the first crack occurrence and read the load increment for each displacement increment during the load application process. In the experiment, as the applied load increases, the cracks gradually extend upwards. When the crack width reaches a certain value and the mid span deflection reaches a certain value, the plate reaches its ultimate load. During the development of cracks, the bending moment at the mid-span is the highest, and as the load increases, the cracks gradually spread towards both sides.

First, cracks developed under loads of 18.7 kN, 13.7 kN, 7.7 kN, and 23.2 kN in JXB1, JXB2, DHB1, and DHB2, respectively. As seen in Figure 17, the crack pattern was already clearly visible when the ultimate load was reached. The mid-span is typically where the first and largest cracks form because it experiences the greatest bending moment. The PIMSP and concrete panel's crack patterns are extremely similar to one another, which is consistent with Ellinna's research on sandwich panels. The JXB2 panel exhibits a similar crack pattern to other panels; however, the absence of truss connections implies that the layers may not be able to be tightly bonded together.

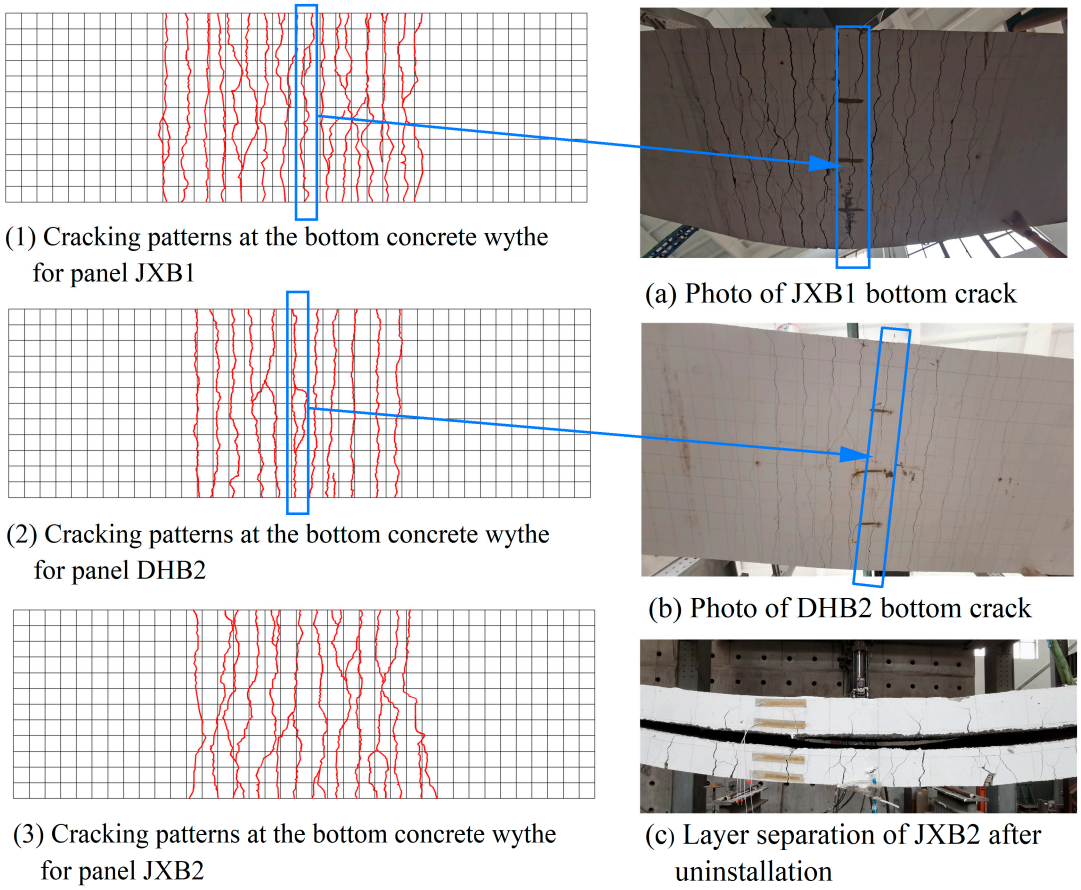


**Figure 17.** Cracking patterns at the bottom concrete wythe for panel JXB1 and DHB2.

## 4. Finite Element Analysis

### *4.1. Form of Finite Element Models*

Discrete models were used to establish the ABAQUS finite element model (FEM), as Figure 18 illustrates. A discrete model is a FEM created by setting up elements for concrete and steel that are sufficiently small and then using the elements' efficient cooperation to create a FEM [30]. While the separated model's calculation results are more accurate and can reveal the interaction mechanism between steel bars and concrete, its slow convergence speed is a drawback.

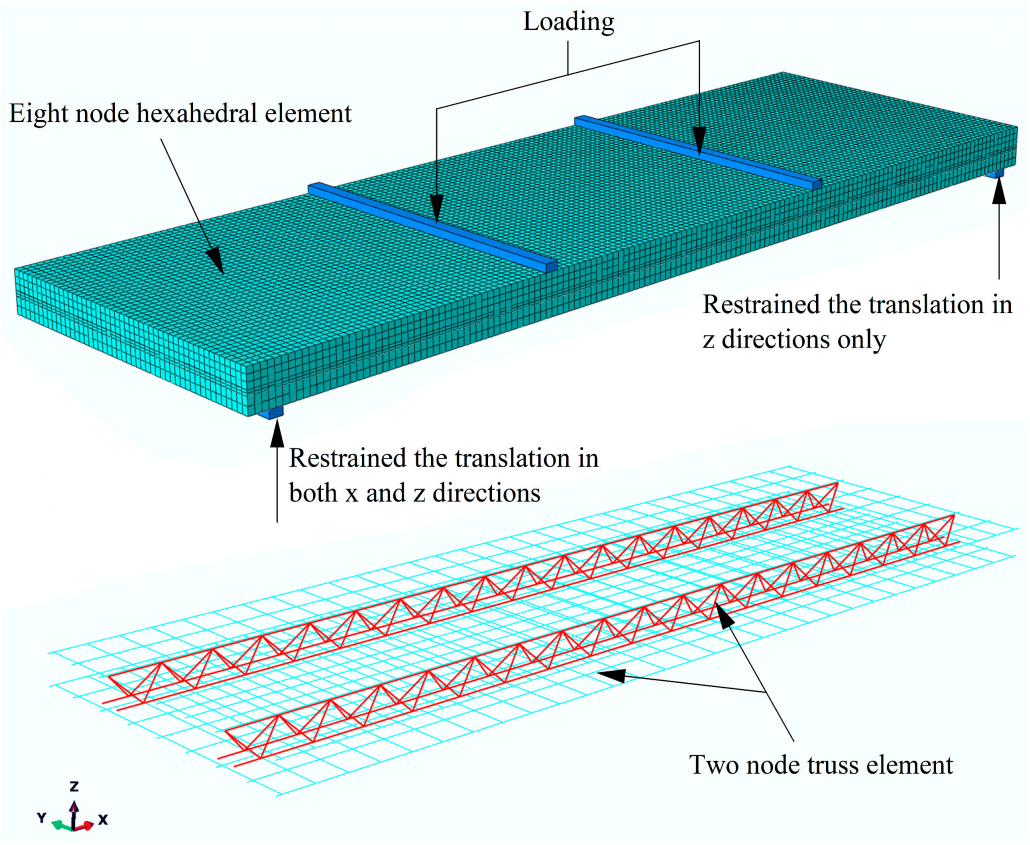


**Figure 18.** ABAQUS finite element model.

*4.2. Typical Elements Used*

Based on the type of component and the expected stress form, two types of element forms were selected: (1) The eight node hexahedral element is mainly used for simulating concrete and insulation mortar, with eight nodes per element and six degrees of freedom per node; (2) The two node truss element is mainly used for simulating steel bars and trusses, with only two nodes per element, and only tensile or compressive strains will occur. Given that the experiment's steel bars and concrete did not exhibit any appreciable slippage, it is assumed that: (1) the sliding of the truss and steel bars is ignored; (2) there is no relative slip between steel bars, trusses, and concrete; and (3) bond slip influence is disregarded [31–33].

*4.3. One-Way PIMSP Slab Model*

Using a three-dimensional continuum, this FEM simulates the behavior of a one-way slab under ideal boundary conditions and loads. In order to match the actual boundary conditions tested, the boundary conditions are set with one end supported by a roller and the other end supported by a hinge. The load is applied on two lines spaced 1300 mm apart, using the same loading mode as the experiment employing displacement loading. To replicate the beams used for loading and support in the experiment, rigid pads were used.

Using an embedded region, which embeds the steel bars and trusses between two layers of concrete panels and insulation layers, limits the space between the steel bars and the concrete. In order to stop the relative movement of overlapping nodes, the insulation layer and the concrete wythes were tied together. A friction coefficient of 0.3 is employed in the tangential direction, and hard contact is used as the normal constraint between the rigid pads and the model.

An effort was made to develop a mesh refinement technique that has good data convergence and does not require a lot of processing power by employing refined mesh refinement optimization and gradually optimizing the mesh. The data will not significantly

change after additional mesh refinement. We divided the grid into distinct sections for each component, ensuring that each had a minimum of two grid divisions in each of the three dimensions.

The majority of the data in the material model uses measured values that are fitted nonlinearly. By entering the measured values into the standard formula, the constitutive model of concrete is computed. By removing a few singular points in accordance with the measured values, the constitutive model of dry-mix mortar is produced. A linear strengthening elastic–plastic model that takes into account the measured yield and limit values is used in the constitutive model of the steel reinforcement. A standardized damage plasticity simulation has been used to add damage plasticity to the concrete material model.

## 5. Comparison of Results

### *5.1. Load-Deflection Profile*

The comparison of mid-span deflection between finite element results and experimental results under different loads is shown in Figure 19. The results show that both the FEA and experimental results exhibit fully composite behavior during the elastic stage, and after cracking, the two exhibit semi-composite behavior. The FEA results' cracking load is only 9% different from the experimental results, and their yield load is 5% higher. Table 4 compares the different load stages of JXB1. The thickness of the insulation layer, the concrete wythes, and the variations in the elastic modulus of the various materials are all taken into consideration by the PIMSP under fully composite behavior when calculating the theoretical values. Therefore, the theoretical value of deflection is the product of applied force and the square of the span at different loading stages, divided by the product of the elastic modulus of the concrete and the moment of inertia of the section.

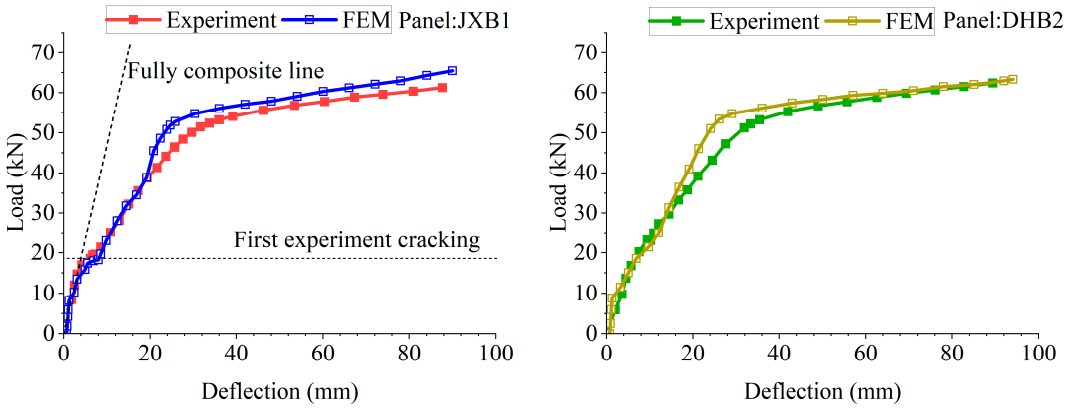


**Figure 19.** Load-deflection profile of mid-span for panels JXB1 and DHB2.

**Table 4.** Comparison of different load stages of JXB1 and DHB2.

| Items | Experiment of JXB1 | FEA of JXB1 | Experiment of DHB2 | FEA of DHB2 |
|---|---|---|---|---|
| 1st cracking load (kN) | 17.0 | 17.5 | 20.3 | 18.6 |
| Increase rate of deflection curve before cracking (mm/kN) | 0.25 | 0.30 | 0.39 | 0.37 |
| Increase rate of deflection curve after cracking (mm/kN) | 0.61 | 0.61 | 0.64 | 0.47 |
| Location of cracking | Mid-span | Mid-span | Mid-span | Mid-span |
| Yield load (kN) | 50.2 | 55.9 | 52.2 | 58.2 |
| Increase rate of deflection curve after yield (mm/kN) | 6.5 | 5.8 | 7.2 | 9.5 |

### *5.2. Strain Distribution*

At the mid-span of the FEM under various loads, the strain distribution along the thickness direction is displayed in Figure 20. There is only one neutral axis in the strain distribution of FEM before it cracks, and it is linear. After cracking, the model exhibits nonlinearity near the sandwich layer, but two neutral axes have not yet appeared, so it is a semi-composite effect at this stage.

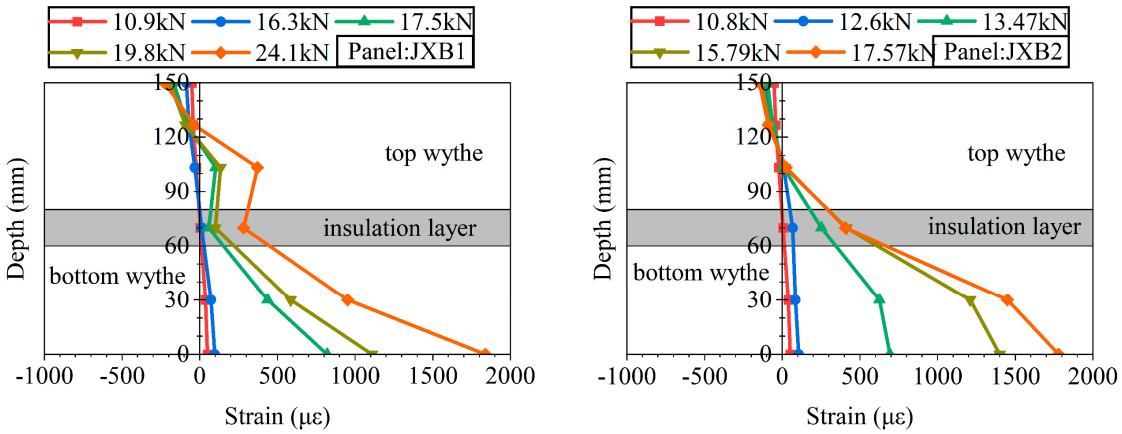


**Figure 20.** Strain distribution across the depth at different load stages for FEM.

### *5.3. Load–Strain Relationship in Steel Bars*

Figure 21 depicts the strain of the steel bars at the bottom of the mid-span based on experimental and FEA results at various loads. The crack load of the FEA results differs from the experimental results by only 9%, and the trend of strain does not change.

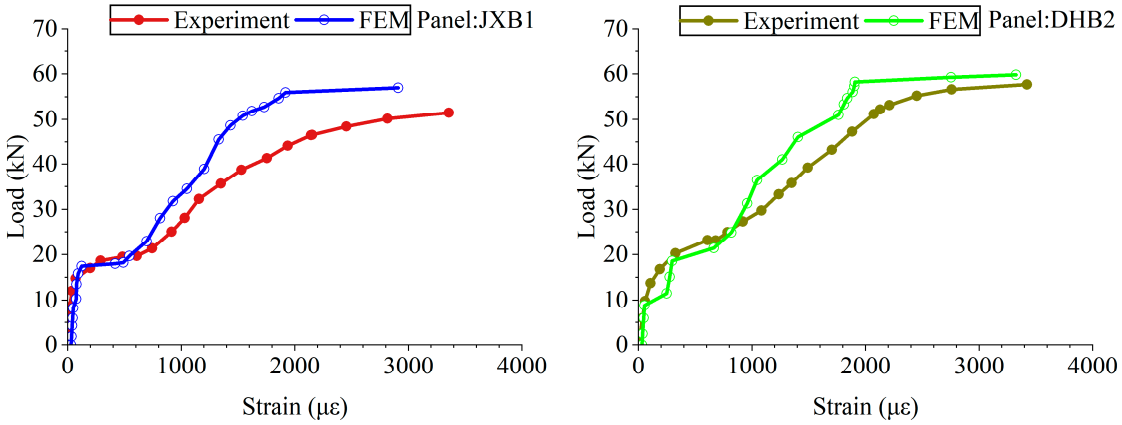


**Figure 21.** Load–strain in steel bars at the mid-span for panels JXB1 and DHB2.

### *5.4. Load–Strain Relationship in Truss Leg*

Comparing the FEM panel with the experimental panel, Figure 22 illustrates the strain in the leg of the panel's mid-span truss. The two curves overlap significantly during the elastic stage. The difference in strain significantly diverged after reaching the first cracking load. The test panel truss leg's strain does not change much until it reaches the yield load, at which point it quickly rises. Following cracking, the leg strain of the finite element plate truss exhibits linear behavior within the interval, increasing uniformly. The force transmitted by the truss web members is demonstrated to be relatively small by both the experimental and finite element results. The difference between the experimental results and the finite element results may be due to the fact that the crack location simulated by the model is not completely consistent with the crack location generated by the experiment,

resulting in a difference in the strain of the truss leg. As a result, the truss leg situation cannot be accurately simulated by the finite element model.

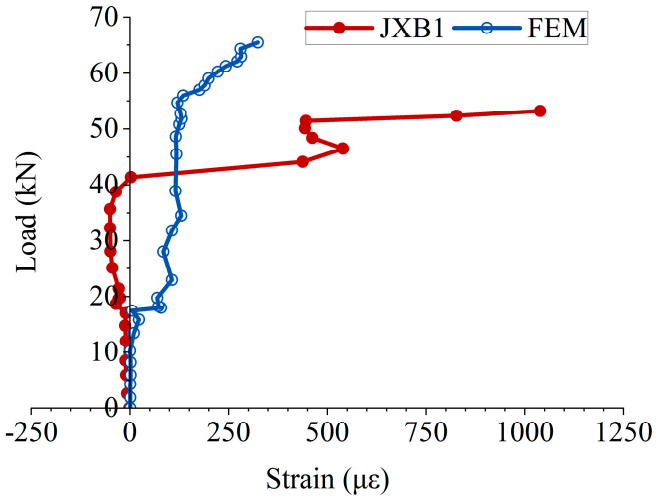


**Figure 22.** Load–strain on the truss leg at mid-span for panel JXB1.

## 6. Conclusions

This paper draws the following conclusions by comparing the experimental and finite element results of two PIMSPs and two concrete slabs:

Compared to the non-truss sandwich insulation composite floor slab, PIMSP has increased its cracking load by 27% and its yield load by 25% due to the introduction of the truss.

In comparison to the concrete slab, the sandwich panel lowers the cracking load by 19% but only by 2% in the yield load under the same thickness. At the same time, PIMSP panels and ordinary concrete slabs have similar cracking patterns.

When the thickness of each layer is the same, the plate JXB1 with a sandwich layer has a 21% higher ultimate load than the plate DHB1 without a sandwich layer, and the cracking period is also later (JXB1 cracks at 37% of the ultimate load, and DHB1 cracks at 19% of the ultimate load).

The PIMSPs and the ordinary composite concrete slabs exhibit consistent cracking patterns during various stages of loading, and the truss coordinates the deformation of the lightweight insulation sandwich layer and the concrete wythes. The sandwich panel achieves a complete composite effect in the elastic stage and a semi-composite effect in the plastic stage.

The results calculated using FEM are significantly consistent with the experimental results, except for the truss web members.

This finite element model can be used as an effective tool for evaluating the composite performance of composite materials in the elastic and plastic stages in the future.

Experiments have shown that PIMSP slabs can replace ordinary concrete slabs as structural components and can reduce material and time consumption for building construction in China's industrialization process.

**Author Contributions:** Conceptualization, M.Z. and B.L.; Methodology, M.Z. and K.C.; Software, W.F. and K.C.; Validation, M.Z. and W.F.; Formal analysis, K.C. and W.F.; Data curation, K.C. and W.F.; Writing—original draft, M.Z. and W.F.; Visualization, M.Z. and W.F.; Funding acquisition, B.L. All authors have read and agreed to the published version of the manuscript.

**Funding:** This research and the APC were funded by Center for Balance Architecture, Zhejiang University, grant number 281410-I5200I.

**Institutional Review Board Statement:** Not applicable.

**Informed Consent Statement:** Not applicable.

**Data Availability Statement:** The original contributions presented in the study are included in the article, further inquiries can be directed to the corresponding author or the first author.

**Acknowledgments:** The authors gratefully acknowledge the financial support for this research from the Center for Balance Architecture, Zhejiang University.

**Conflicts of Interest:** Authors Mingshan Zhang, Kepeng Chen and Benyue Li were employed by the company The Architectural Design & Research Institute of Zhejiang University Corporation Limited. The remaining author declare that the research was conducted in the absence of any commercial or financial relationships that could be construed as a potential conflict of interest.

## References

1. Einea, A. Structural and Thermal Efficiency of Precast Concrete Sandwich Panel Systems. 1992. Available online: https://api.semanticscholar.org/CorpusID:138315946 (accessed on 11 April 2023).
2. Einea, A.; Salmon, D.C.; Fogarasi, G.J.; Culp, T.D.; Tadros, M.K. State-of-the-Art of Precast Concrete Sandwich Panels. *PCI J.* **1991**, *36*, 78–98. [CrossRef]
3. Amran, Y.H.M.; Rashid, R.S.M.; Hejazi, F.; Safiee, N.A.; Ali, A.A.A. Response of precast foamed concrete sandwich panels to flexural loading. *J. Build. Eng.* **2016**, *7*, 143–158. [CrossRef]
4. Einea, A.; Salmon, D.C.; Tadros, M.K.; Culp, T.D. A new structurally and thermally efficient precast sandwich panel system. *PCI J.* **1994**, *39*, 90–101. [CrossRef]
5. Losch, E.D.; Hynes, P.W.; Andrews, R., Jr.; Browning, R.; Cardone, P.; Devalapura, R.; Donahey, R.; Freedman, S.; Gleich, H.A.; Goettsche, G.; et al. State of the art of precast/prestressed concrete sandwich wall panels. *PCI J.* **2011**, *56*, 131–176.
6. Benayoune, A.; Samad, A.A.A.; Trikha, D.N.; Ali, A. Buckling Characteristics of Precast Concrete Sandwich Wall Panels. In Proceedings of the 2nd Word Engineering Congress, Sarawak, Malaysia, 1 January 2002.
7. Mohamad, N.; Hassan, N. The Structural Performance of Precast Lightweight Foam Concrete Sandwich Panel with Single and Double Shear Truss Connectors Subjected to Axial Load. *Adv. Mater. Res.* **2013**, *634–638*, 2746–2751. [CrossRef]
8. Joseph, J.D.R.; Prabakar, J.; Alagusundaramoorthy, P. Experimental studies on through-thickness shear behavior of EPS based precast concrete sandwich panels with truss shear connectors. *Compos. Part B Eng.* **2019**, *166*, 446–456. Available online: https://api.semanticscholar.org/CorpusID:140002852 (accessed on 11 April 2023). [CrossRef]
9. Jiang, H.; Guo, Z.; Liu, J.; Liu, H. The Shear Behavior of Precast Concrete Sandwich Panels with W-shaped SGFRP Shear Connectors. *KSCE J. Civ. Eng.* **2018**, *22*, 3961–3971. [CrossRef]
10. Yang, X.; Liu, H.X.; Cheng, W. Experimental Study on Flexural Property of Precast Cavity Concrete Sandwich Wall Panels. In *IOP Conference Series: Earth and Environmental Science*; IOP Publishing: Bristol, UK, 2020; Volume 508. Available online: https://api.semanticscholar.org/CorpusID:225618962 (accessed on 19 April 2023).
11. Zhai, X.; Ying, W.; Xueming, W. Experimental Study on Shear Performance of New Composite Connector for Precast Concrete Sandwich Panels. 2017. Available online: https://api.semanticscholar.org/CorpusID:114028138 (accessed on 19 April 2023).
12. Luebke, J.; Pozo-Lora, F.F.; Al-Rubaye, S.; Maguire, M. Out-of-Plane Flexural Behavior of Insulated Wall Panels Constructed with Large Insulation Thicknesses. *Materials* **2023**, *16*, 4160. Available online: https://api.semanticscholar.org/CorpusID:259049147 (accessed on 17 February 2024).
13. Arevalo, S.I.; Tomlinson, D. Experimental thermal bowing response of precast concrete insulated wall panels with stiff shear connectors and simple supports. *J. Build. Eng.* **2020**, *30*, 101319. [CrossRef]
14. Pozo-Lora, F.F.; Maguire, M. Thermal bowing of concrete sandwich panels with flexible shear connectors. *J. Build. Eng.* **2020**, *29*, 101124. [CrossRef]
15. Bush, T.D.; Wu, Z.M. Flexural analysis of prestressed concrete sandwich panels with truss connectors. *PCI J.* **1998**, *43*, 76–86. [CrossRef]
16. Pfeifer, D.W.; Hanson, J.A. Precast Concrete Wall Panels: Flexural Stiffness of Sandwich Panels. 1965. Available online: https://api.semanticscholar.org/CorpusID:138027186 (accessed on 11 April 2023).
17. Joseph, J.D.R.; Prabakar, J.; Alagusundaramoorthy, P. Precast concrete sandwich one-way slabs under flexural loading. *Eng. Struct.* **2017**, *138*, 447–457. [CrossRef]
18. Hu, X. Characteristics and Application of Thermal Mortar Materials in Building Materials. *Mater. Today Proc.* **2020**, *22*, 2539–2543. [CrossRef]
19. Bai, F.; Sun, Y.; Liu, X.; Li, X. A theoretical perspective on the effective distribution of shear connectors in sandwich structure. *Compos. Struct.* **2021**, *272*, 114139. [CrossRef]
20. Cox, B.; Syndergaard, P.; Al-Rubaye, S.; Pozo-Lora, F.F.; Tawadrous, R.; Maguire, M. Lumped GFRP star connector system for partial composite action in insulated precast concrete sandwich panels. *Compos. Struct.* **2019**, *229*, 111465. [CrossRef]
21. Salmon, D.C.; Einea, A. Partially Composite Sandwich Panel Deflections. *J. Struct. Eng.* **1995**, *121*, 778–783. [CrossRef]
22. Benayoune, A.; Samad, A.A.A.; Trikha, D.N.; Ali, A.A.A.; Ellinna, S.H.M. Flexural behaviour of pre-cast concrete sandwich composite panel—Experimental and theoretical investigations. *Constr. Build. Mater.* **2008**, *22*, 580–592. [CrossRef]

23. O'Hegarty, R.; Kinnane, O. Review of precast concrete sandwich panels and their innovations. *Constr. Build. Mater.* **2020**, *233*, 117145. [CrossRef]
24. Tawil, H.B.; Tan, C.G.; Sulong, N.H.R.; Nazri, F.M.; Sherif, M.M.; El-Shafie, A.S. Mechanical and Thermal Properties of Composite Precast Concrete Sandwich Panels: A Review. *Buildings* **2022**, *12*, 1429. Available online: https://api.semanticscholar.org/CorpusID:252265720 (accessed on 15 May 2023). [CrossRef]
25. West, R.P.; Kinnane, O. Composite Behaviour of Thin Precast Concrete Sandwich Panels. 2021. Available online: https://api.semanticscholar.org/CorpusID:236649807 (accessed on 15 May 2023).
26. Mlynarczyk, A.J.; Pessiki, S.P. Experimental Evaluation of the Composite Behavior of Precast Concrete Sandwich Wall Panels. *PCI J.* **2003**, *48*, 54–71.
27. Bush, T.D.; Stine, G.L. Flexural behavior of composite precast concrete sandwich panels with continuous truss connectors. *PCI J.* **1994**, *39*, 112–121. [CrossRef]
28. Choi, I.-H.; Kim, J.; Kim, H.-R. Composite Behavior of Insulated Concrete Sandwich Wall Panels Subjected to Wind Pressure and Suction. *Materials* **2015**, *8*, 1264–1282. [CrossRef]
29. Chris, P.P.; Rajeev, S.; Lawrence, D.R. Structural Performance of Hybrid GFRP/Steel Concrete Sandwich Panels. *J. Compos. Constr.* **2008**, *12*, 570–576. [CrossRef]
30. Gara, F.; Ragni, L.; Roia, D.; Dezi, L. Experimental behaviour and numerical analysis of floor sandwich panels. *Eng. Struct.* **2012**, *36*, 258–269. [CrossRef]
31. Huang, Q.; Hamed, E. Nonlinear finite element analysis of composite precast concrete sandwich panels made with diagonal FRP bar connectors. *Compos. Struct.* **2019**, *212*, 304–316. [CrossRef]
32. Suidan, M.; Schnobrich, W.C. Finite Element Analysis of Reinforced Concrete. *J. Struct. Div.* **2019**, *99*, 2109–2122. [CrossRef]
33. Yaman, T.S.; Lucier, G.W. Shear Transfer Mechanism between CFRP Grid and EPS Rigid Foam Insulation of Precast Concrete Sandwich Panels. *Buildings* **2023**, *13*, 928. Available online: https://api.semanticscholar.org/CorpusID:257887540 (accessed on 11 April 2023). [CrossRef]


**Disclaimer/Publisher's Note:** The statements, opinions and data contained in all publications are solely those of the individual author(s) and contributor(s) and not of MDPI and/or the editor(s). MDPI and/or the editor(s) disclaim responsibility for any injury to people or property resulting from any ideas, methods, instructions or products referred to in the content.